Proceedings of the XXXIXth Rencontres de Moriond
Series: Moriond Workshops
La Thuile, Italy January 25 - February 1st, 2004

QUANTUM INFORMATION AND DECOHERENCE IN NANOSYSTEMS

edited by

D. Christian Glattli

Marc Sanquer

Jean Trân Thanh Vân

THẾ GIỚI
PUBLISHERS

Sponsored by

. CNRS (Centre National de la Recherche Scientifique) - Formation permanente.
. CEA (Commissariat à l'Énergie Atomique) - Direction des sciences de la matière : DRFMC (Grenoble) et DRECAM (Saclay).

Thế Giới Publishers
Printed in Vietnam
GPXB: 1-1325/XB-QLXB (16-9-2004)
VN-TG-11325.1

XXXIXth Rencontres de Moriond
La Thuile, Aosta Valley, Italy - January 25 - February 1st, 2004

Quantum Information and Decoherence in Nanosystems
Series: Moriond Workshops

UNIVERSAL REGIME OF FIDELITY DECAY IN REALISTIC QUANTUM COMPUTATIONS

KLAUS M. FRAHM, ROBERT FLECKINGER, DIMA L. SHEPELYANSKY
Laboratoire de Physique Théorique, UMR 5152 du CNRS,
Université Paul Sabatier, 31062 Toulouse Cedex 4, France

We determine the universal scaling law for fidelity decay in quantum computations of complex dynamics in presence of internal static imperfections in a quantum computer. Based on random matrix theory we show that this decay is governed by an exponential decay with Fermi's golden rule decay rate for time scales smaller than the Heisenberg time and a gaussian decay for larger time scales. The theoretical predictions are tested and confirmed in extensive numerical simulations of a quantum algorithm for quantum chaos in the dynamical tent map with up to 18 qubits and with ten orders of magnitude for the relevant scaled fidelity interval.

Recently a great deal of attention has been attracted [1,2,3] to the problem of quantum computation. A quantum computer is viewed as a system of qubits. Each qubit can be considered as a two-level quantum system, *e.g.* one-half spin in a magnetic field. For n_q qubits the whole system is characterized by a finite-dimensional Hilbert space with $N = 2^{n_q}$ quantum states. It has been shown that all unitary operations in this space can be realized with certain elementary quantum gates [3,4] acting on one or two particular qubits. A quantum computation can be much faster than a classical one due the massive parallelism of many-body quantum mechanics since any step of a quantum evolution is a multiplication of a vector by a unitary matrix. There are computational algorithms that can be represented as a sequence of such elementary gates involving only a polynomial number (in n_q) of gates such as the Shor algorithm [5] for factorization of integers with n_q digits, the Grover algorithm [6] for a search in an unstructured database and the quantum Fourier transform [1,3] (QFT). With the help of QFT the quantum evolution of certain many-body quantum systems can be performed in a polynomial number of gates [7,8]. Other examples can be found in the evolution of quantum dynamical systems which are chaotic in the classical limit [9,10]. Such systems are described by chaotic quantum maps and include the quantum baker map [11], the quantum kicked rotator [12], the quantum saw-tooth map [13] and the quantum double-well map [14]. We furthermore mention the quantum simulation of the Anderson metal-insulator transition [15] and the study of classical chaotic dynamics where quantum computation provides a more effecient access to some new information. [16,17]

For potential experimental implementations of a quantum computer one has to take into account errors caused either by decoherence induced by unavoidable couplings to external world [18] or by internal static imperfections inside the quantum computer. These static imperfections generate residual couplings between qubits and variation of energy level-spacing from one qubit to another. Such imperfections lead to emergence of many-body quantum chaos in a quantum computer hardware if a coupling strength exceeds a quantum chaos threshold. [19] To analyze the effects of errors one may consider the fidelity f defined as $f(t) = | < \psi_{\rm err}(t)|\psi(t) > |^2$ where $|\psi(t) >$ is the quantum state at time t computed with perfect (or ideal) gates, while $|\psi_{\rm err}(t) >$ is the quantum state at time t computed with errors. If the fidelity is close to unity then a quantum computation with imperfections is close to the ideal one while if f is significantly smaller than 1 then the computation gives, generally, wrong results. The fidelity decay for generic quantum evolution with different models of dynamical evolution and perturbations has attracted a considerable interest over the last years (see *e.g.* [20,21] and references therein). In this work we consider the fidelity decay in quantum computation due to static imperfections a case previously studied only in a few works. [13,22,21] We present analytical results of a random matrix approach valid for a regime of complex quantum dynamics and a numerical study of a particular quantum map with 18 qubits.

We consider a kicked rotator whose classical dynamics is governed by the map,

$$\begin{array}{rcl} \bar{p} & = & p - V'(\theta) \\ \bar{\theta} & = & \theta + \bar{p}T \ (\bmod\ 2\pi) \end{array} \quad , \quad V(\theta) = \begin{cases} -\frac{k}{2}\theta(\theta-\pi) & , \quad 0 \le \theta < \pi \\ \frac{k}{2}(\theta-\pi)(\theta-2\pi) & , \quad \pi \le \theta < 2\pi \end{cases} \tag{1}$$

Here the kick-potential $V(\theta)$ is composed of two parabolic pieces. The parameter k determines the kick strength and T gives the rotation of phase between kicks. This map is similar in structure to the Chirikov standard map.[24] The derivative $V'(\theta)$ has a tent form and is continuous but not differentiable at $\theta = 0$ and $\theta = \pi$. This is an intermediate case between the standard map[24] with a perfectly smooth kick-potential and the saw-tooth map[13] with a non-continuous potential derivative. The dynamics of the classical tent map (1) depends only on one dimensionless parameter $K = kT$, its properties have been studied in [25,26]. For small values of K the dynamics is governed by a KAM-scenario with the Kolmogorov-Arnold-Moser (KAM) invariant curves and a stable island at $\theta = 3\pi/2$, $p = 0$ and a chaotic layer around separatrix starting from the unstable fixed point (saddle) at $\theta = \pi/2$, $p = 0$. At $K = 4/3$, the last invariant curve is destroyed and one observes a transition to global chaos with a mixed phase space containing big regions with regular dynamics.[25,26,21] In the following, we are particularly interested in a typical case $K = 1.7$, which exhibits global chaos with quite large stable islands in phase space related to the main and secondary resonances.

The quantized version of the classical map (1) is given by the unitary quantum map,

$$|\psi(t+1)\rangle = U\,|\psi(t)\rangle = e^{-iT\hat{p}^2/2}\,e^{-iV(\hat{\theta})}\,|\psi(t)\rangle\,. \tag{2}$$

where the $|\psi(t)\rangle$ is the quantum state at the (integer) time t and the variables $\hat{p}$ and $\hat{\theta}$ are operators with the commutator $[\hat{p},\hat{\theta}] = -i$. They have integer eigenvalues p for $\hat{p}$ and real eigenvalues θ in the interval $[0, 2\pi[$ for $\hat{\theta}$. Furthermore $\hbar = 1$ and the quasiclassical limit correspond to $T \to 0$, $k \to \infty$ with $K = kT = const.$ For the quantum dynamics we concentrate our studies on the case $K = kT = 1.7$ and $T = 2\pi/N$ that corresponds to the evolution on one classical cell (see Fig. 1) with N quantum states.

The quantum map (2) can be efficiently simulated on a quantum computer. For this we represent the quantum state $|\psi(t)\rangle$ by a quantum register with n_q qubits with a total number of $N = 2^{n_q}$ different basis states. The eigenstates of $|p\rangle$ of $\hat{p}$ are identified with the quantum register states $|\alpha_0\rangle_0\,|\alpha_1\rangle_1 \ldots |\alpha_{n_q-1}\rangle_{n_q-1}$ with $p = \sum_{j=0}^{n_q-1} \alpha_j 2^j \in \{0, \ldots, N-1\}$ and $\alpha_j \in \{0, 1\}$. Here $|0\rangle_j$ and $|1\rangle_j$ correspond to the two basis states of the j-th qubit.

For quantum computations one typically assumes that the quantum computer can be constructed with quantum gates that manipulate at most two qubits such as the simple phase-shift, controlled phase-shift, controlled-NOT and the Hadamar gate.[3,4] Without entering into the details we mention that it is possible[21] to express the unitary operator U in the quantum map (2) in terms of $n_g = \frac{9}{2}n_q^2 - \frac{11}{2}n_q + 4$ elementary quantum gates. For a moderate number of qubits ($n_q = 10 \sim 20$) it is possible to test the quantum algorithm on a classical computer.[21] For example in the first and third panel of Fig. 1, we show the density plot of the Husimi function of a quantum state which was obtained by such a quantum computation of the quantum map (2) after a large number of iterations. As an initial state we have used a minimal coherent wave packet placed in the chaotic or integrable component (near the unstable fix point at $\theta = \pi/2$, $p = 0$ for the first panel and in the main stable island at $\theta = 5.35$, $p = 0$ for the third panel). In both cases the classical behavior is well reproduced, i. e. in the first case the chaotic region is ergodically filled up while for the regular initial condition the wave packet stays close to the classical invariant curve.

We have investigated the stability of the quantum algorithm for the tent map with respect to errors. For this we note that quantum algorithm of the tent map[21] is given by the expression $U = \prod_{j=1}^{n_g} U_j$ where U_j are the unitary operators associated to the elementary gates and n_g is

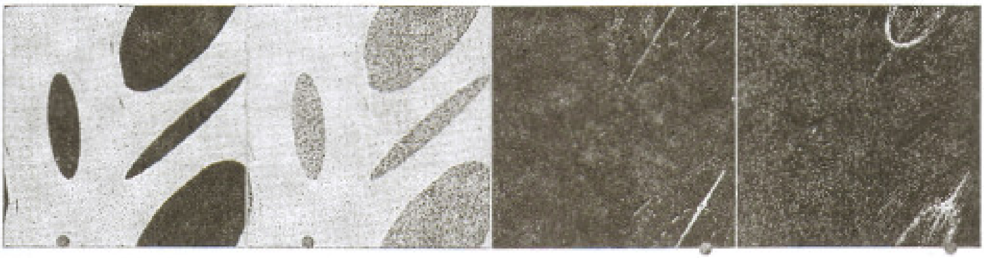

Figure 1: Density plots of the Husimi functions of the quantum state $|\psi(t)>$ with an initial state $|\psi(0)>$ chosen as a minimal coherent (gaussian) wave packet located at the positions of the red/grey circles. The first and second panels (from left to right) correspond to the iteration number $t = 5625$, qubit number $n_q = 16$ and to a chaotic initial condition closely located to the saddle at $\theta = \pi/2$, $p = 0$. The third and fourth panels correspond to $t = 22783$, $n_q = 14$ and to a regular initial condition at $\theta = 5.35$, $p = 0$. The second and fourth panels are obtained from a quantum computation with static errors with $\epsilon = 7 \cdot 10^{-7}$, fidelity $f = 0.9388$ (second panel) and $\epsilon = 5 \cdot 10^{-7}$, fidelity $f = 0.5$ (fourth panel). The density is minimal for blue/black and maximal for red/white. The dashed line in the third panel correponds to the invariant curve to which the classical trajectory is restricted.

the number of these gates. The errors are modelized by the replacement $U_j \to U_j\, e^{i\delta H_j}$ where δH_j is a hermitian operator representing a perturbation. There are two models of imperfections. The first one represents random noise errors in quantum gates fluctuating in time from one gate to another with $\delta H_j \sim \varepsilon$ random and different at each j and t. In this case the fidelity decay is clearly exponential [21] for very long time scales, $f(t) = \exp(-t/t_r)$ with $t_r = 1/(0.095\varepsilon^2 n_q^2)$. The second model describes only static imperfections. [19,13,22,15] In this case we chose $\delta H_j = \delta H$ independant of j and t with : $\delta H = \sum_{j=0}^{n_q-1} \delta_j\, \sigma_j^{(z)} + 2\sum_{j=0}^{n_q-2} J_j\, \sigma_j^{(x)}\, \sigma_{j+1}^{(x)}$ where $\sigma_j^{(\nu)}$ are the Pauli matrices acting on the jth qubit and $\delta_j,\ J_j \in [-\sqrt{3}\varepsilon, \sqrt{3}\varepsilon]$ are random coefficients which are drawn only once at the beginning and kept fixed during the simulation. In the second and fourth panel of Fig. 1 we show the Husimi functions of two quantum states obtained by a quantum computation with such static imperfections.

We now introduce the effective operator δH_{eff} for the full static error at one complete iteration with the quantum map (2) by: $\prod_{j=1}^{n_g}(U_j\, e^{i\delta H}) = U\, e^{i\delta H_{\text{eff}}}$. As it was shown by Prosen et al. [20], in the limit $(1-f) \ll 1$ one can express the fidelity in terms of a correlation function, [20,21]

$$f(t) \approx 1 - \frac{t}{t_c} - \frac{2}{t_c}\sum_{\tau=1}^{t-1}(t-\tau)\, C(\tau) \quad , \quad C(\tau) = t_c\, \langle U^{-\tau}\delta H_{\text{eff}} U^{\tau}\delta H_{\text{eff}}\rangle\rangle_Q \ . \tag{3}$$

Here $\langle\langle\cdots\rangle\rangle_Q$ denotes the quantum expectation value and the time scale $t_c = 1/\langle\langle(\delta H_{\text{eff}}{}^2)\rangle\rangle_Q$ ensures the normalisation $C(0) = 1$ of the correlation function.

For an initial state in the chaotic region we may assume that the unitary quantum map U can be modeled by a random matrix drawn from Dyson's circular orthogonal ensemble. [23] Performing the ensemble average with respect to U, we obtain the following scaling expression for the fidelity: [21]

$$-\langle \ln f(t)\rangle_U \approx \frac{N}{t_c}\chi\left(\frac{t}{N}\right) \quad , \quad \chi(s) \approx s + 2\, s^2 \quad \Rightarrow \quad f(t) \approx \exp\left(-\frac{t}{t_c} - \frac{2}{\sigma}\frac{t^2}{t_c t_{\text{H}}}\right) \tag{4}$$

where N corresponds to the number of "chaotic" states fixing the dimension of the random matrix U. In (4) we have replaced $N = \sigma\, t_{\text{H}}$ where σ is the fraction of the chaotic part of phase space ($\sigma \approx 0.65$ for $K = 1.7$) This result gives a clear transition from exponential to gaussian decay at $t \approx t_{\text{H}}$ if $t_c \ll t_{\text{H}}$. If $t_c \gg t_{\text{H}}$ the exponential regime is barely visible and dominated by the gaussian decay. We have numerically verified this scaling behavior for n_q between 6 and 18, for ε between 10^{-4} and $5 \cdot 10^{-7}$ and for 10 orders of magnitude of the rescaled fidelity (see Fig. 2). We have performed a scaling analysis of the fidelity for the chaotic and regular initial condition.

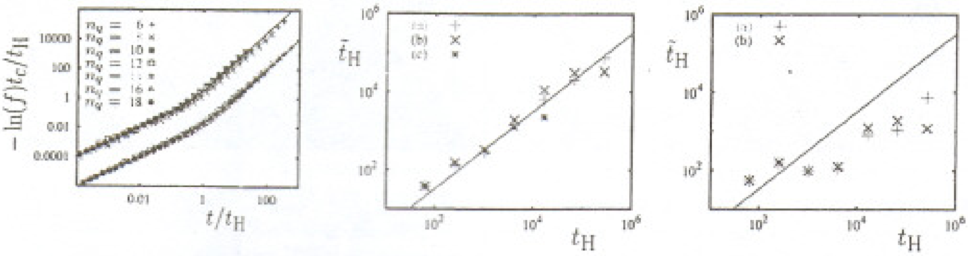

Figure 2: **Left:** scaling representation of the fidelity f for the initial condition in the chaotic region. The upper scaling curve shows: $-\ln(f)t_c/t_H$ as a function of t/t_H with the two theoretical time scales $t_c = (\varepsilon^2 n_q n_g^2)^{-1}$ and $t_H = 2^{n_q}$. The full line in the upper curve corresponds to the scaling curve (4). The lower scaling curve (shifted down by a factor 0.01) correspond to $-\ln(f)\tilde{t}_c/\tilde{t}_H$ versus $t/\tilde{t}_H$ with the times scales $\tilde{t}_c$ and $\tilde{t}_H$ obtained from the fit $y = x + x^2$ (with $y = -\ln(f)\tilde{t}_c/\tilde{t}_H$ and $x = t/\tilde{t}_H$) for each value of n_q and ε. Full line is $y = x + x^2$. **Middle:** $\tilde{t}_H$ versus t_H for the chaotic initial condition for $6 \leq n_q \leq 18$, $\varepsilon = 5 \cdot 10^{-7}$ [data points (a)] and $\varepsilon = 10^{-5}$ [data points (b)]. The data points (c) are obtained from an ensemble average over 200 realizations of static imperfections for each value of $n_q = 6, 8, 10, 12, 14$ and $\varepsilon = 5 \cdot 10^{-7}$ The full line corresponds to the theoretical expression $\tilde{t}_H = (\sigma/2)t_H$. **Right:** $\tilde{t}_H$ versus t_H for the initial condition in the integrable region.

In particular, we have determined for each value of n_q and ε two time scales $\tilde{t}_c$ and $\tilde{t}_H$ by a numerical least square fit of $\ln(f(t)) = -t/\tilde{t}_c - t^2/(\tilde{t}_c\tilde{t}_H)$ (with appropriate weight factors. [21]) We find that for both types of initial conditions this fit works quite well and that the first time scale $\tilde{t}_c$ coincides quite well with its theoretical expression: [21] $t_c \approx 1/(\varepsilon^2 n_q n_g^2)$. The situation is different for the second time scale $\tilde{t}_H$ which coincides with its theoretical value $(\sigma/2)\, t_H$ only for the chaotic initial condition (see middle and right part of Fig. 2). This observation is in agreement with a natural expectation that random matrix theory is not applicable to regular dynamics.

The scaling result (4) provides a universal description of the fidelity decay in quantum algorithms simulating complex dynamics on a realistic quantum computer with static imperfections. This decay determines the time scale t_f of reliable quantum computation [defined by $f(t_f) = 0.9$] according to $t_f \approx t_c/10$ for $t_H > t_c$ [corresponding to $\varepsilon > \varepsilon_{ch} = 2^{-n_q/2}/(n_g\sqrt{n_q})$] or $t_f \approx 0.2\sqrt{t_c t_H}$ for $t_H < t_c$ ($\varepsilon < \varepsilon_{ch}$). Therefore the total number of gates which can be performed with fidelity $f > 0.9$ is given by $N_g = t_f n_g \approx 1/(10\varepsilon^2 n_q n_g)$ (for $\varepsilon > \varepsilon_{ch}$) or $N_g \approx 2^{n_q/2}/(5\varepsilon\sqrt{n_q})$ (for $\varepsilon < \varepsilon_{ch}$). The first case compares to the behavior for random errors [21] $N_g \approx 5/\varepsilon^2$ with the same dependence on ε while the second case, which may be dominant for 10-15 qubits, is completely different. This difference should play an important role for the quantum error correction codes. [2,3]

This work was supported in part by the EC IST-FET project EDIQIP and the NSA and ARDA under ARO contract No. DAAD19-01-1-0553 and by the French goverment grant ACI Nanosciences-Nanotechnologies LOGIQUANT. We thank CalMiP at Toulouse and IDRIS at Orsay for access to their supercomputers.

References

1. A. Ekert and R. Josza, Rev. of Mod. Phys. **68**, 733 (1996).
2. A. Steane, Rep. Prog. Phys. **61**, 117 (1998).
3. M.A. Nielsen and I.L. Chuang *Quantum Computation and Quantum Information*, Cambridge Univ. Press, Cambridge (2000).

4. D. P. Di Vincenzo, Science **270**, 255 (1995).
5. P.W. Shor, in *Proc. 35th Annual Symposium on Foundation of Computer Science*, Ed. S.Goldwasser (IEEE Computer Society, Los Alamitos, CA, 1994), p.124
6. L. K. Grover, Phys. Rev. Lett. **79**, 325 (1997).
7. S. Lloyd, Science **273**, 1073 (1996).
8. G. Ortiz, J.E. Gubernatis, E. Knill, and R.Laflamme, Phys. Rev. A **64**, 22319 (2001).
9. B.V.Chirikov, F.M.Izrailev and D.L.Shepelyansky, Sov. Scient. Rev. C (Gordon & Bridge) **2**, 209 (1981); Physica D **33**, 77 (1988).
10. F.M.Izrailev, Phys. Rep. **196**, 299 (1990).
11. R. Schack, Phys. Rev. A **57**, 1634 (1998).
12. B. Georgeot, and D.L. Shepelyansky, Phys. Rev. Lett. **86**, 2890 (2001).
13. G. Benenti, G. Casati, S. Montangero, and D.L. Shepelyansky, Phys. Rev. Lett. **87**, 227901 (2001).
14. A.D. Chepelianskii and D.L. Shepelyansky, Phys. Rev. A **66**, 054301 (2002).
15. A.A. Pomeransky and D.L. Shepelyansky, Phys. Rev. A **69**, 014302 (2004).
16. B. Georgeot and D.L. Shepelyansky, Phys. Rev. Lett. **86**, 5393 (2001); **ibid. 88**, 219802 (2002).
17. M. Terraneo, B. Georgeot and D.L. Shepelyansky, Eur. Phys. J. D **22**, 127 (2003).
18. W.H. Zurek, Rev. Mod. Phys. **75**, 715 (2003).
19. B.Georgeot and D.L.Shepelyansky, Phys. Rev. E **62**, 3504 (2000); **62**, 6366 (2000).
20. T. Prosen, T.H. Seligman and M. Znidaric, Prog. Theor. Phys. Supp. **150**, 200 (2003); T. Gorin, T. Prosen, and T. H. Seligman, preprint nlin. CD/0311022.
21. K.M. Frahm, R. Fleckinger and D.L. Shepelyansky, Eur. Phys. J. D **29**, 139 (2004).
22. M. Terraneo and D.L. Shepelyansky, Phys. Rev. Lett. **90**, 257902 (2003).
23. T. Guhr, A. Mueller-Groeling and H.A. Weidenmueller, Phys. Rep. **299**, 189 (1998).
24. B.V. Chirikov, Phys. Rep. **52**, 263 (1979).
25. S. Bullett, Com. Math. Phys. **107**, 241 (1986).
26. V.V. Vecheslavov, Zh. Eksp. Teor. Fiz. **119**, 853 (2001) (nlin.CD/0005048); V.V. Vecheslavov and B.V. Chirikov, Zh. Eksp. Teor. Fiz. **120**, 740 (2001) (nlin.CD/0202017).